Temperature and Pressure Insensitive Spectroscopic Method for Measuring $^{13}CH_4$ during Oil and Natural Gas Drilling Operations

Guolin Li*, Qingzhi Jiang, Chenquan Hua, Kun Ma, Yue Jiao and Wenhai Ji

College of and Control Science and Engineering, China University of Petroleum, Qingdao, China

A novel rugged two-section driving NIR TDLAS scheme was implemented to reduce temperature and pressure sensitivity of methane carbon isotope measurement during oil and natural gas drilling operations. Isotope spectra line groups with same lower energy levels were selected to derive the concentration of $^{13}CH_4$ and $^{12}CH_4$. Dynamic pressure linewidth broadening was introduced in the absorbance curve fitting. Various uncontrollable factors such as spectra shift, stretching, and baseline trending were incorporated in the comprehensive multi-peak fitting. The results showed that the sensitivity of isotope ratios to temperature and pressure variation was greatly suppressed. The $\delta^{13}CH_4$ uncertainty in the temperature test was 2.8‰ with fitted $\delta^{13}CH_4$-T slope of 0.021‰/°C in 25 ± 5°C range. The $\delta^{13}CH_4$ uncertainty in the pressure test was 1.4‰ with fitted $\delta^{13}CH_4$-P slope of <0.001‰/mbar from 400 to 1000 mbar. The limit standard deviation of long-term test was 0.15‰ (@135 s). The results indicate that our scheme is a promising solution for $\delta^{13}CH_4$ measurement during drilling operations due to the enhanced robustness.

Keywords: TDLAS, pressure insensitive, temperature insensitive, isotope ratios, two-section driving, multi-peak fitting

INTRODUCTION

The natural gases' carbon isotopes composition provides an effective basis for quantitatively describing the migration, transformation, and traceability of chemical substances in oil and gas resources [1–5]. Therefore, it is necessary to develop an efficient and stable technique for *in situ* detecting the carbon isotopes during oil and natural gas drilling operations [6, 7]. Isotopic abundance can be expressed as the relative ratio between the heavy isotopic component and the light isotopic components. $\delta^{13}CH_4$ is determined by measuring the concentration ratio of $^{13}CH_4$ and $^{12}CH_4$. The $\delta^{13}CH_4$ detection in the drilling site requires *in situ* measurement, robustness in the harsh operating conditions, and better than 1‰ accuracy.

Various spectroscopic techniques have been investigated for carbon isotope detection, including Fourier transform infrared spectroscopy (FTIR) [8], tunable diode laser absorption spectroscopy (TDLAS), off-axis integrated cavity output spectroscopy (OA-ICOS) [9–11], and cavity ring-down spectroscopy (CRDS) [12]. Nixon *et al.* measured the Mars' satellite Titan's $\delta^{13}CH_4$ with ±83‰ uncertainty by using FTIR [13], which is due to the incoherence of broadband light in FTIR. OA-ICOS and CRDS were used to measure $\delta^{13}CH_4$ in atmospheric background methane with an accuracy of 1–2‰ [14, 15]. Even the sensitivity is high, the $\delta^{13}CH_4$ values were extremely sensitive to

gas temperature and pressure. For example, 1‰ $\delta^{13}CH_4$ accuracy requires temperature < ±50 mK and pressure <±1.33 mbar [16].

Other spectroscopic $\delta^{13}CH_4$ measurement in trace environmental methane used mid-infrared lasers such as interband cascade laser (ICL) [16], nonlinear differential frequency generation (DFG) through $LiNO_3$ crystal [17, 18], with accuracy ranging from 0.7‰ to 12‰. Due to increased optical pathlength in multiple reflection gas cell, tunable diode laser absorption spectroscopy (TDLAS) with NIR laser is feasible to measure $\delta^{13}CH_4$ in natural gas. In 2019, Zhang *et al.* used a 1.658 µm DFB laser to detect $\delta^{13}CH_4$ in coal bed methane (CBM) and achieved standard deviation of 0.47‰ [19]. However, their control accuracy of temperature and pressure was very tight, i.e., P < ±1 mbar and T < ±0.05 K.

Thus, the temperature and pressure sensitivities are common issues of current spectroscopic isotope measurement techniques which hinder their applications in drilling operations. In present work, we proposed a novel single laser TDLAS technique by selecting isotope spectral lines with the same lower energy level to suppress the temperature variation impact on absorption strength. In addition, two-section laser driving, and comprehensive multi-peak fitting model were used to compensate the pressure dependence. The experimental result was around 1‰ precision without tight control of temperature and pressure.

Selection of Isotope Spectra Lines

Concentration of gaseous $^{13}CH_4$ and $^{12}CH_4$ can be derived through their absorption spectra based on Beer-Lambert's Law. When selecting $^{13}CH_4$ and $^{12}CH_4$ absorption spectral lines near 1.65 µm through HITRAN2016 database [20], the line separation, line strength, and temperature sensitivity should be considered. Eventually, four lines of 5E, F→6E, F transition belonging to the $2\nu_3$ R5 line were chosen for $^{13}CH_4$, listed as A1-A4 in **Table 1** and plotted in **Figure 1** (blue A1-A4 dots). Two lines of 5F2,1→5F1,2 transition belonging to the $2\nu_3$ Q5 line were chosen for $^{12}CH_4$, listed as B1-B2 in **Table 1** and plotted in **Figure 1** (red B1-B2 dots). They are ~1.8 nm apart, which is close to the tuning limit of a DFB laser. For spectral strength, the line strength of $^{12}CH_4$ is about twice of $^{13}CH_4$ under natural abundance. Thus, the $^{12}CH_4$ spectra

provide a stable reference for measuring the $^{13}CH_4$ spectra and concentration of subtle isotope variation. The lower level vibration quantum numbers of A and B lines are (0,0,0,0), the rotational quantum numbers are 5, and the energies are ~157.1 cm^{-1}. Thus, the influence of temperature on the absorption spectra is canceled per Boltzmann distribution. The detection result is insensitive to temperature variation. The candidate spectral lines A and B with important spectral parameters are shown in **Table 1**. Besides A and B lines, suboptimal $^{12}CH_4$ candidate lines C1-C2 with least spectral interference are also listed in **Table 1** and plotted in **Figure 1**(red C1-C2 dots). Three congested $^{12}CH_4$ peaks at 6046.94, 6046.95, and 6046.96 cm^{-1} with corresponding 3F, A→4F, A transitions belonging to the $2\nu_3$ R4 line are located in the middle of the wavelength range, listed in **Table 1** as O1-O3. Their line intensities are 2–3 orders of magnitude stronger, which are out of **Figure 1** scope.

Spectroscopy Theory for Isotope Measurement

Isotopic abundance can be expressed as the relative ratio between the heavy isotopic component and the light isotopic components. For example, the carbon isotope abundance value (^{13}C) of a sample can be described by $\delta^{13}C$ [4] i.e.,

$$\delta^{13}C = \left(\frac{(13_C/12_C)_{Sample}}{(13_C/12_C)_{PDB}} - 1 \right) \times 1000‰ \qquad (1)$$

Where, $(^{13}C/^{12}C)_{Sample}$ is the concentration ratio ^{13}C to ^{12}C of test sample; $(^{13}C/^{12}C)_{PDB}$ is the ratio of standard substance- Pee Dee Belemnite. By definition, $\delta^{13}C$ for PDB is 0, and the corresponding $^{13}C:^{12}C$ ratio is 0.01118. $\delta^{13}CH_4$ was determined by measuring the concentrations of $^{13}CH_4$ and $^{12}CH_4$. The concentration was derived by fitting the absorbance curve which was transformed from the normalized transmission spectra [20].

The target test sample is natural gas. But only its major component methane is used in our experiment for simplicity. The tested methane was in a 30 L stainless steel cylinder at a starting pressure of 1500 psi and was provided by Yantai Deyi Specialty Gas. Before we ran the spectra test, gas was sampled twice and was analyzed by a Thermo Fisher Scientific isotope analyzing system consisting of TRACE1310

TABLE 1 | The spectral parameters of $^{13}CH_4$ and $^{12}CH_4$ candidate lines.

No	Molecule	Transition center/(cm^{-1})	Line intensity (cm-1/(mole·cm^{-2}))	Lower state energy/(cm^{-1})	Upper state quanta	Lower state quanta
B1	$^{12}CH_4$	**6042.42**	**1.61E-23**	**157.1243**	**NA**	**0 0 0 0 1A1**
B2	$^{12}CH_4$	**6042.52**	**1.81E-23**	**157.1279**	**0 0 2 0 E**	**0 0 0 0 1A1**
C1	$^{12}CH_4$	6044.12	6.43E-24	10.4817	NA	0 0 0 0 1A1
C2	$^{12}CH_4$	6044.28	1.16E-24	815.0000	NA	NA
O1	$^{12}CH_4$	6046.94	7.88E-22	62.8758	NA	0 0 0 0 1A1
O2	$^{12}CH_4$	6046.95	9.28E-22	62.8768	NA	0 0 0 0 1A1
O3	$^{12}CH_4$	6046.96	1.46E-21	62.8782	0 0 2 0 F2	0 0 0 0 1A1
A1	$^{13}CH_4$	**6049.12**	**8.63E-24**	**157.1316**	**0 0 2 0 F2**	**0 0 0 0 1A1**
A2	$^{13}CH_4$	**6049.16**	**8.56E-24**	**157.1352**	**0 0 2 0 F2**	**0 0 0 0 1A1**
A3	$^{13}CH_4$	**6049.23**	**5.96E-24**	**157.1445**	**0 0 2 0 F2**	**0 0 0 0 1A1**
A4	$^{13}CH_4$	**6049.24**	**8.12E-24**	**157.1462**	**0 0 2 0 F2**	**0 0 0 0 1A1**

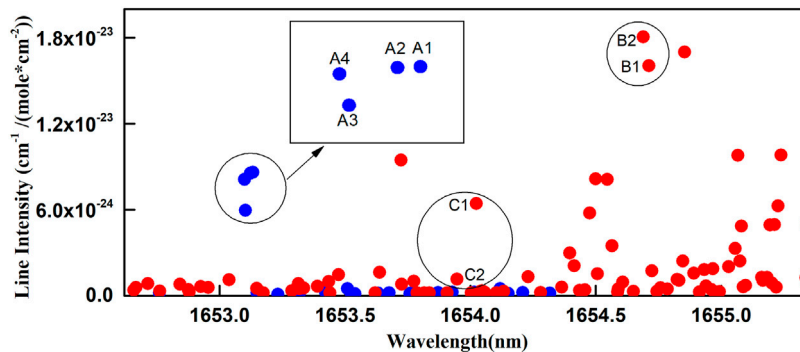*Bold values indicate absorption lines with the same low-level energy.*

FIGURE 1 | The line intensity plot of CH_4 in the $2v_3$ absorption band. The red dots are for $^{12}CH_4$ and the blue dots are for $^{13}CH_4$ with insets indicating detailed view.

gas chromatograph (GC) and MAT 253 PLUS mass spectrometer (MS). The average $\delta^{13}CH_4$ values after 4–5 analysis were −41.04‰ and −41.01‰ which provided the basis to calibrate the accuracy of present spectroscopic method.

EXPERIMENTAL APPARATUS

Experiment Setup

The experiment was carried out in an automatic gas mixing station (**Figure 2**) which was controlled through a LabVIEW program. The station consists of mass flow controllers (MFC, Sevenstar CS200), pressure controller (PC, TESCOM ER5000), vacuum pump and temperature chamber. The gas cell was placed inside the temperature chamber where experiment can run from 0 to 50°C. The MFCs' ranges are in 100–5000 SCCM with an accuracy of 1%. The pressure range is 400–1000 mbar with an accuracy of about 2 mbar. The tests ran automatically with different gas mixture in four dimensions including flow rate, ratio, temperature and pressure.

The TDLAS apparatus' scheme is shown in **Figure 3**. A butterfly NIR DFB diode laser (Wuhan 69 Sensors, SN18020801) was used for direct absorption measurement. The wavelength scan was controlled by a periodical waveform current to cover both the target absorption lines of $^{13}CH_4$ and $^{12}CH_4$. The laser output was coupled into a multi-pass Chernin cell with 20 m pathlength through its pigtail fiber. A built in InGaAs photon detector was used to collect the transmitted light. The detector signal went through I-V conversion and low-pass filtering before analog digital convertor (DAC) acquisition.

By using Hewlett Packard 86120B wavelength meter and Fabry-Perot (F-P) scanning interferometer (SA210-12B) to study the tuning parameters of the laser, the tuning curve is shown in **Figure 4**. The current tuning coefficient and temperature tuning coefficient of the laser are 0.03025 nm/mA and 0.0699 nm/°C respectively. The average wavelength-current tuning coefficient is larger than that of ordinary DFB lasers (typically 0.005–0.01 nm/mA). This laser diode was specifically chosen for its large tuning coefficient, so that all target absorption lines of $^{13}CH_4$ and $^{12}CH_4$ were covered.

In order to verify the stability of the laser light source, the laser temperature was stabilized at 34.3°C and the driving current were set at 25–35 mA and 90–116 mA, the stability of the absorption spectrum of the laser light intensity absorbed by 10% methane gas has been researched, the test time was 1 h, and extracted 100 absorption spectra, as shown in **Figure 2**. The maximum deviation was 0.0847, so it is indirectly proved that the laser has good stability.

Two-Section Driving of DFB Laser

However, there are still challenges in spectra analysis due to the following reasons. First, there are lots of lines in between the two target line groups and some lines are adjacent to the target lines
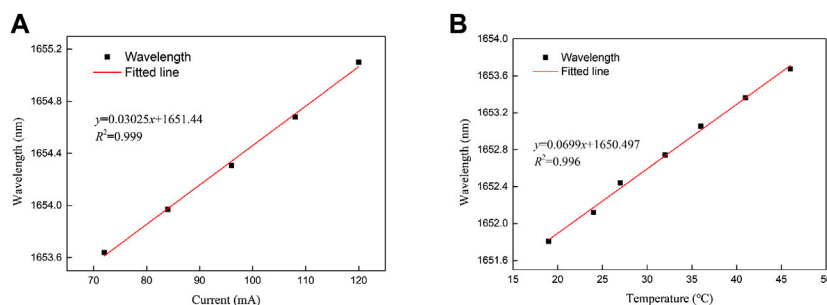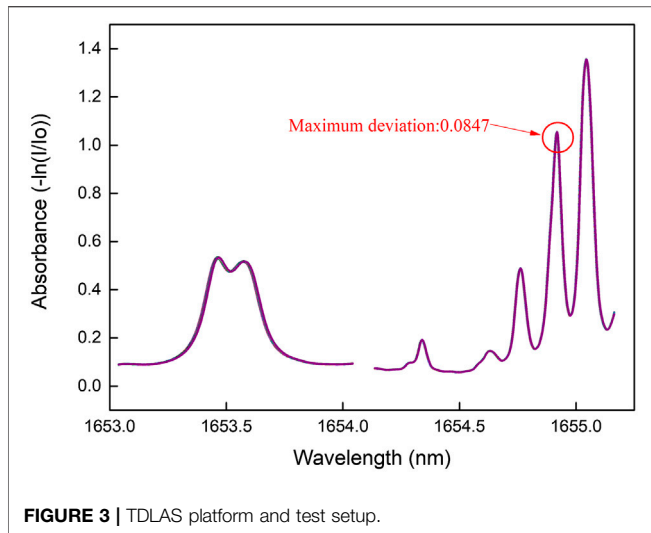

FIGURE 2 | The stability of the absorption spectrum of the laser light intensity absorbed by 10% methane gas.

FIGURE 3 | TDLAS platform and test setup.

(**Figure 1** insets). Second, there is strong linearity due to the large wavelength separation (**Figure 4**). Thus, it brings extra uncertainty in absorbance calculation. There is too much trivial information in the collected spectra for continuous nonstop scan (**Figure 5A**).

A two-section current driving scheme was proposed and implemented to address these challenges. In this scheme, the two isotope target spectra lines were aimed by two sections of driving current (I_1 = 25–35 mA, I_2 = 90–100 mA) at laser operating T of 34.3°C (**Figure 5B**). The overall scan period was 200 ms. The strong peak in conventional one large section (I = 25–100 mA) driving scheme (**Figure 5A** O) was eliminated. As a result, the spectra gain setting is now restricted by the target lines rather than by the strong background lines, which increase

the spectra signal strength by more 100 times. In addition, the data length representing target lines increased from 260 points to approximately 900 points, with resolution increased 3.5 times. Thus, the features in experimental absorbance have better resemblance with HITRAN2016 simulated absorbance. The wavelength linearity in each section was also improved.

Spectra Preprocess

In order to improve the signal to noise ratio of spectra, the spectra were averaged after every 10 scans. In order to calculate the absorbance, the transmitted light I_0 with no absorbing gas (pure nitrogen) in the cell was collected and was used as the normalization basis. When the sample gas was guided into the cell, real time transmitted light I_s was collected. In each section, the absorbance curve A_i was calculated separately.

$$A_i = -\ln\left(\frac{I_{si}}{I_{oi}}\right) \qquad (2)$$

Where, i = 1,2 is the current section index, I_{si}, I_{oi} are the transmitted light power in the ith section with and without absorbing gases.

Multi-Peak Fitting

For the temperature and pressure range in the experiment, a Gaussian waveshape was adopted in the absorbance spectra fitting. In fact, there are more peaks in the absorbance curve other than the target peaks in the designated section. A multi-peak fitting model was introduced,

$$\varphi(x) = \sum_{j=1}^{2} \sum_{i=1}^{m} \frac{1}{\sigma_i \sqrt{2\pi}} C_j S_i^j e^{\left(-\frac{(x-\mu_i)^2}{2\sigma_i^2}\right)} \qquad (3)$$
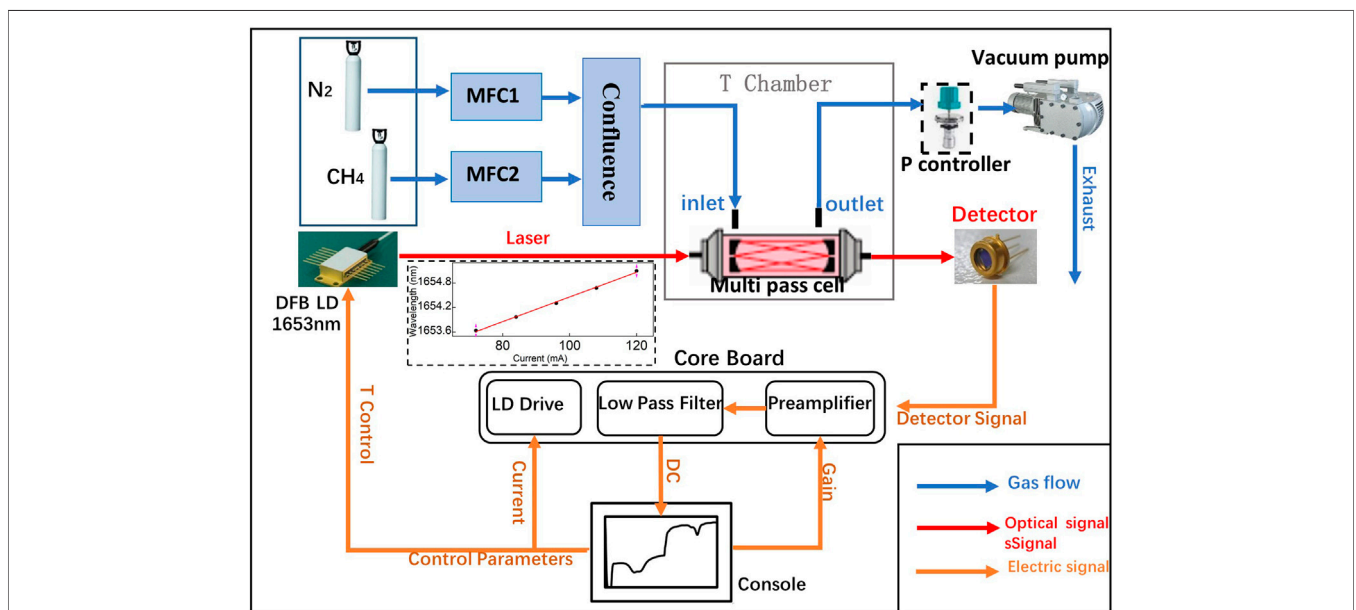

FIGURE 4 | (A) Laser current tuning curve **(B)** Laser temperature tuning curve.

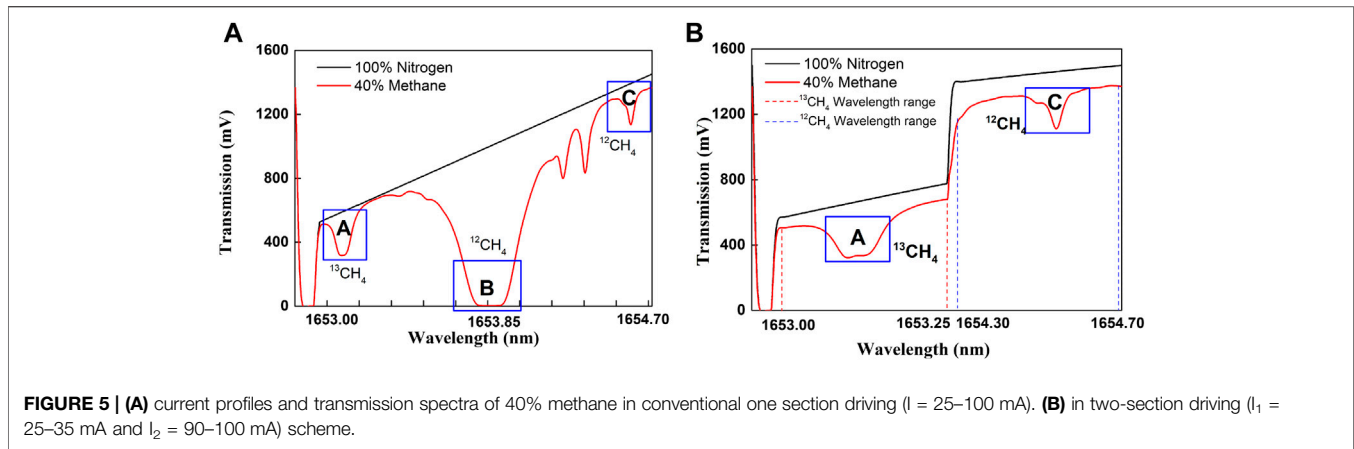**FIGURE 5 | (A)** current profiles and transmission spectra of 40% methane in conventional one section driving (I = 25–100 mA). **(B)** in two-section driving (I$_1$ = 25–35 mA and I$_2$ = 90–100 mA) scheme.

Where, C_j (j = 1,2) is the coefficients proportional to the $^{13}CH_4$ and $^{12}CH_4$ concentration and is further used to calculate $\delta^{13}CH_4$, S_i^j is the absorbance strength of the ith line of the jth isotope molecules, μ_i is the center wavelength of the ith line, σ_i is the linewidth of ith line, m is total number of lines. In order to improve the fitting accuracy, all lines listed in HITRAN2016 including the weak ones were included. Based on the HITRAN2016 database, the self-broadening coefficient of all absorption lines within the scanning range of the laser is almost similar to the pressure broadening coefficient, all of which are in the same order of magnitude. In particular, the self-broadening coefficient of the target absorption line is completely same with the pressure broadening coefficient. Even if the line width of the absorption line is slightly different, it is negligible. So the linewidth of ith line (σ_i) was kept constant.

The initial values of the peak center, line width, line amplitude and line separations are linearly related to the spectral parameters in HITRAN2016. There is a scale transformation from the database with absolute wavelength to experimental spectra with discrete data points by,

$$\mu_i = \mu_1 + bh_i \qquad (4)$$

Where, μ_1 is the position of first peak in the experimental absorbance curve, h_i is the wavelength difference in database between the ith line and the first line, b is the scale transformation coefficients. By this formula, the spectra shift the horizontal direction can be automatically adjusted and compensated.

However, there are many practical factors affecting the performance in experiment. Due to laser/detector aging, gas flow turbulence, mirror contamination or optical alignment change, thermal drift of amplifier's gain, there are uncontrollable fluctuations in the transmitted light, which will result in the whole absorbance curve upward or downward shift. The strong nonlinear wavelength-current relation causes the nonlinear shift (i.e., stretch) of the absorbance spectra. Furthermore, there is also nonlinear detector response at different laser power level which makes the absorbance curve having a trending baseline. So, we have to build a comprehensive fitting model by introducing more parameters,

$$\varphi(x) = \sum_{j=1}^{2} \sum_{i=1}^{m} \frac{1}{\sigma_i \sqrt{2\pi}} C_j S_i^j e^{\left(-\frac{(x+k_1 x - \mu_i)^2}{2\sigma_i^2}\right)} + k_2 x + c \qquad (5)$$

Where, the extra terms c, $k_1 x$, and $k_2 x$ are used to compensate baseline trending, horizontal scale stretching and the vertical shift in the absorbance curve. The curve fitting model was implemented in a MATLAB program. The detection accuracy of $\delta^{13}C$ is determined by **Eq. 5**. The parameters that affect the error of comprehensive fitting model $\varphi(x)$ mainly include fitting coefficients (C_j), absorbance strength of the ith line the jth isotope molecules (S_i^j), the center wavelength of the ith line (μ_i) the linewidth of ith line (σ_i), total number of lines(m), baseline trending(c), horizontal scale stretching ($k_1 x$) and vertical shift ($k_2 x$). Among the above parameters, absorbance strength of the ith line the jth isotope molecules (S_i^j) can be found in HITRAN2016 database, and the rest of variables are need to be determined. In order to reduce the error, the relative positions of all the target absorption peaks from the HITRAN2016 database were obtained. So once the center wavelength of the ith line (μ_i) was determined, and so on, the other center wavelength of the lines were determined. The remaining variables change within a certain range, so that comprehensive fitting model $\varphi(x)$ is very close to the collected absorption spectrum, so as to determine the optimal value of the variable. The optimal fitting coefficients were obtained iteratively with multiple nonlinear constraints. The fitting result is demonstrated in **Figure 6**. The transmitted light with and without absorbing gas in two sections are shown in (a). The calculated absorbance and model fitted absorbance in two sections are shown in (b). The spectra fitting residue was 1% of the signal amplitude and shown in (c). After the fitting coefficients C_j were obtained, their ratio is correlated to the concentration ratio in **Eq. 1** by the GC-MS analysis of test sample. For a selected sample, the ratio should remain constant under any conditions. Thus, the repeatability and robustness against environmental factors' variation are important indicators of the measurement techniques.
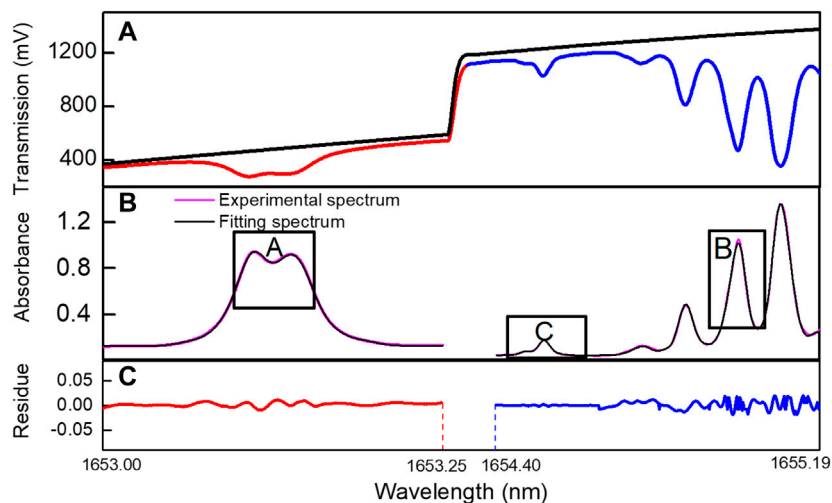
FIGURE 6 | Spectra analysis process: **(A)** the transmitted light I$_0$ and I$_s$; **(B)** the absorbance curve; **(C)** the spectra fitting residue.

EXPERIMENTS AND RESULTS

The isotope ratio measurement performance was experimentally evaluated in terms of temperature sensitivity, pressure sensitivity and repeatability. The experimental details are listed in **Table 2**. The repeatability was characterized by standard deviation of δ^{13}CH$_4$ in the long-term test. The spectroscopic ratio values of 10% CH$_4$ at 25°C, 400 mbar were used as the reference, corresponding to δ^{13}CH$_4$ of −41.04‰.

Pressure Dependence

Simulated absorbance curves for each wavelength region at 400, 700, and 1000 mbar based on the HITRAN2016 are plotted in **Figures 7A,B**. As a comparison, the experimental absorbance curves from pressure test are plotted in **Figures 7C,D** for each driving section. The Simulated absorbance curve for ^{13}CH$_4$ and ^{12}CH$_4$ data are derived from HITRAN2016, the carbon isotope abundance value (δ^{13}C) for simulation data is different from δ^{13}C for the experimental data. Thus, simulated absorbance curve for ^{13}CH$_4$ and ^{12}CH$_4$ do not agree with experimental absorbance curve for ^{13}CH$_4$ and ^{12}CH$_4$ in **Figure 7**. As the pressure changes, the pressure broadening effect becomes more obvious. With the decrease of the pressure, the full width at half maximum of absorbance curve for ^{13}CH$_4$ and ^{12}CH$_4$ decreases gradually. Absorption spectrum mixing effect is less apparent. Thus, experiment running at lower pressure can help to improve δ^{13}C detection accuracy.

To extend pressure range coverage, the pressure broadened linewidth was included in the curve fitting **Eq. 4**. The linewidth for each peak was calculated by,

$$\sigma = P \times \left(nCH_4 \times \delta_{self} + nN_2 \times \delta_{air} \right) \qquad (6)$$

Where, P is gas pressure in ATM, nCH_4 and nN_2 are the relative concentrations of methane and nitrogen in the gas mixture, δ_{self} and δ_{air} are self and air pressure broadening coefficients from HITRAN2016. For the selected ^{13}CH$_4$ spectra lines, their self and air broadening coefficients are 0.06 and 0.077 cm^{-1}/ATM. For the selected ^{12}CH$_4$ spectra lines (Choice B), their self and air broadening coefficients are 0.066 and 0.077 cm^{-1}/ATM. The δ^{13}CH$_4$ in the pressure test is plotted in **Figure 8**. The standard deviation for the overall test is 1.4‰ (**Figure 8A**). The δ^{13}CH$_4$ shows no pressure dependence with linear fit slope <0.001‰/mbar (**Figure 8B**). Introduction of dynamic pressure linewidth broadening by **Eq. 5** is the key to maintain good δ^{13}CH$_4$ accuracy in pressure test.

Temperature Dependence

For the two choices of measuring ^{12}CH$_4$, choice B is the target line with same lower energy levels, but it is congested with other lines. Choice C is more isolated and less affected by the interference. As a comparison, we used both choices to fit the coefficients of ^{12}CH$_4$. The calculated δ^{13}CH$_4$ during temperature test with same flowing gas for choice B and C was plotted in **Figure 8C** red and blue curve. The choice C is clearly more sensitive to temperature change. The

TABLE 2 | Experimental protocol table.

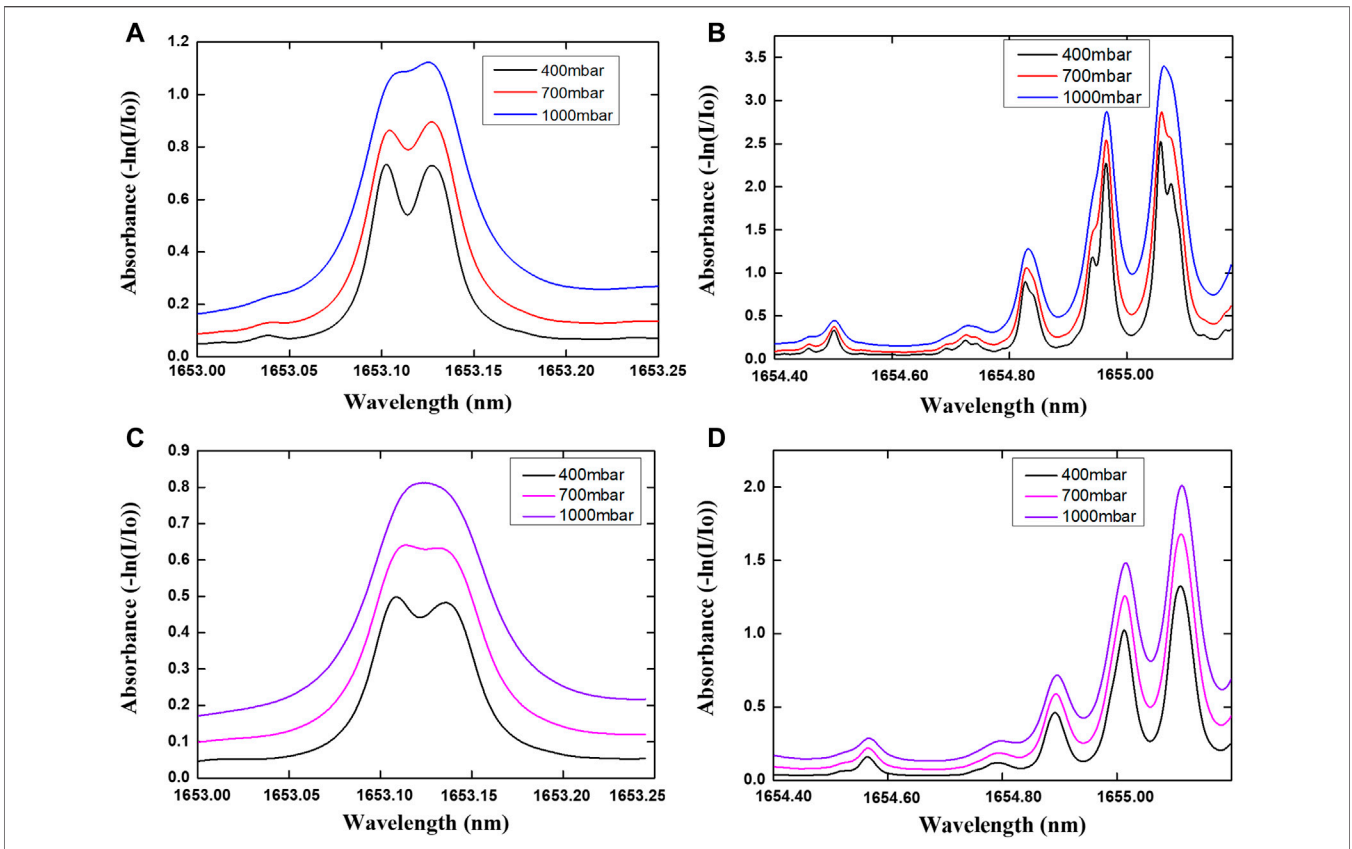| Conditions type	Gas mixture	Pressure	Temperature	Duration
Pressure test	10%CH$_4$ + 90%N$_2$	400–1000 mbar By 100 mbar incremental	25°C	10 min each
Temperature test	10%CH$_4$ + 90%N$_2$	400 mbar	20°C, 25°C, 30°C	150 min each
Long term test	10%CH$_4$ + 90%N$_2$	400 mbar	25°C	180 min

FIGURE 7 | The experimental and simulation absorbance curves of 10% CH_4 and 90% N_2 in each section at 400, 700, 1000 mbar pressures: (A) HITRAN2016 Simulated absorbance curve for $^{13}CH_4$ and (B) for $^{12}CH_4$; (C) Experimental absorbance curve for $^{13}CH_4$ and (D) for $^{12}CH_4$.
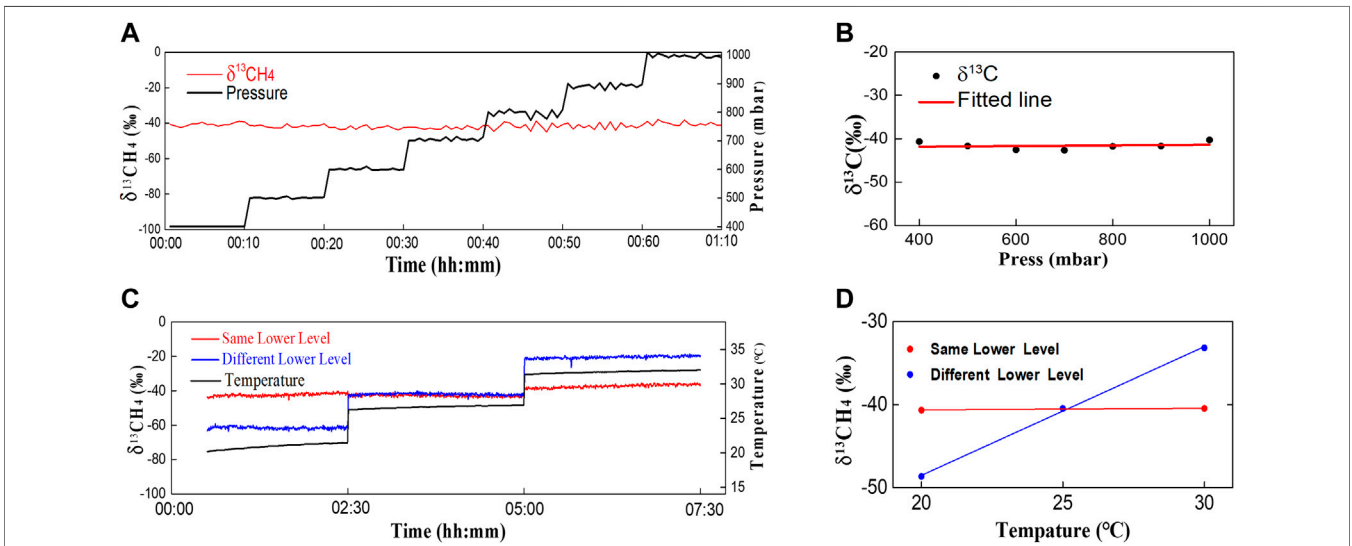

FIGURE 8 | $\delta^{13}CH_4$ in the pressure and temperature sensitivity test. (A) $\delta^{13}CH_4$ and pressure reading in pressure test; (B) $\delta^{13}CH_4$-pressure dependence analysis; (C) $\delta^{13}CH_4$ and temperature reading in temperature test for choice B (red) and choice C (blue); (D) $\delta^{13}CH_4$ -temperature dependence analysis for choice B (red) and choice C (blue).

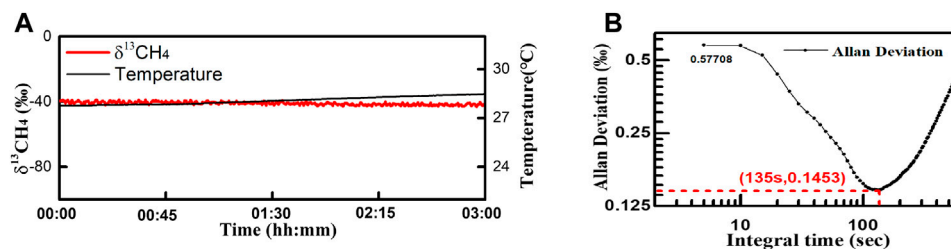**FIGURE 9 | (A)** Long term test of $\delta^{13}CH_4$ and **(B)** Allan analysis.

standard deviations in the whole test are 2.8‰ and 16.9‰ for choice B and C respectively. The linear fitting slope of $\delta^{13}CH_4$ - temperature curve for choice B (**Figure 8D** red curve) is 0.021‰/°C which is 2 orders weaker than that of choice C (1.55‰/°C, **Figure 8D** blue curve). This proved that the selection of same lower energy state was more effective than spectra interference in terms of reducing temperature dependence.

Long Term Test

During the 3-hour long term test, the gas cell was placed inside the test chamber with T set at 25°C. The pressure was maintained at 400 mbar. The gas mixture of 10% CH_4 and 90% N_2 flowed through the cell at 100 ml/min rate. Totally 500 spectra were collected. We applied the multi-peak Gaussian waveshape fitting with absorbance curve. The calculated $\delta^{13}CH_4$ are plotted in **Figure 9A** with standard deviation of 0.95‰ at update time of 2 s. Allan analysis of $\delta^{13}CH_4$ measurement in long-term test gives the limit standard deviation is 0.14‰ (@135 s) (**Figure 9B**).

CONCLUSION

We proposed and implemented a rugged two-section laser driving TDLAS system in which a broad tuning NIR DFB laser was used to cover spectra lines for both isotope molecules. Isotope spectra lines with same lower energy levels were selected to derive the $^{13}CH_4$ and $^{12}CH_4$ concentrations. In addition to dynamic pressure broadening linewidth, various uncontrollable factors such as spectra shift, stretching, and trending were addressed in the comprehensive multi-peak absorbance curve fitting by introducing the corresponding terms.

The $\delta^{13}CH_4$ uncertainty in the temperature test was 2.8‰ with fitted $\delta^{13}CH_4$ - temperature slope of 0.021‰/°C in 25 ±

5°C range. The $\delta^{13}CH_4$ uncertainty in the pressure test was 1.4‰ with fitted $\delta^{13}CH_4$ - pressure slope of <0.001‰/mbar from 400 to 1000 mbar. The limit standard deviation of long-term test was 0.15‰ (@135 s). The $\delta^{13}CH_4$ precisions of a few research groups were better. But their apparatuses were more complicated and delicate mainly due to stringent requirement of pressure and temperature control. Our NIR TDLAS scheme is a promising solution for $\delta^{13}CH_4$ measurement during drilling operations.

DATA AVAILABILITY STATEMENT

The original contributions presented in the study are included in the article/Supplementary Material, further inquiries can be directed to the corresponding author.

AUTHOR CONTRIBUTIONS

Writing—original draft preparation, GL; writing—review and editing GL and QJ; methodology, CH; software, KM; data curation, YJ and WJ; All authors have read and agreed to the published version of the manuscript.

FUNDING

REFERENCES

1. Bastviken D, Tranvik LJ, Downing JA, Crill PM, Enrich-Prast A Freshwater methane emissions offset the continental carbon sink. *Science* (2011) 331:50. doi:10.1126/science.1196808

2. Turnbull JC, Karion A, Fischer ML, Faloona I, Lehman SJ, Miller BR, et al. Assessment of fossil fuel carbon dioxide and other anthropogenic trace gas emissions from airborne measurements over Sacramento, California in

spring 2009. *Atmos Chem Phys* (2011) 11:705–21. doi:10.5194/acp-11-705-2011

3. Graham WM, Condon RH, Carmichael RH, D'Ambra I, Patterson HK, Linn LJ, et al. Oil carbon entered the coastal planktonic food web during the Deepwater Horizon oil spill. *Environ Res Lett* (2010) 5:045301. doi:10.1088/1748-9326/5/4/045301

4. Mohn J, Werner RA, Buchmann B, Emmenegger L High-precision δ^{13} CO_2 analysis by FTIR spectroscopy using a novel calibration strategy. *J Mol Struct* (2007) 834:95–101. doi:10.1088/1748-9326/5/4/045301

5. Cao JJ, Chow JC, Tao J, Lee SC, Watson JG, Ho KF, et al. Stable carbon isotopes in aerosols from Chinese cities: influence of fossil fuels. *Atmos Environ* (2011) 45:1359–63. doi:10.1088/1748-9326/5/4/045301

6. Zhang K, Meng ZP, Wang XM Distribution of methane carbon isotope and its significance on CBM accumulation of No.2 coal seam in Yanchuannan CBM block, Ordos Basin, China. *J Pet Sci Eng* (2019) 174:92–105. doi:10.1088/1748-9326/5/4/045301

7. Li Y, Tang DZ, Fang Y, Xu H, Meng Y Distribution of stable carbon isotope in coalbed methane from the east margin of Ordos Basin. *Sci China-Earth Sci* (2014) 57:1741–8. doi:10.1007/s11430-014-4900-x

8. Li GL, Dong ET, Ji WH A near-infrared trace CO_2 detection system based on an 1,580 nm tunable diode laser using a cascaded integrator comb (CIC) filter-assisted wavelength modulation technique and a digital lock-in amplifier. *Front Phys* (2019) 7:199. doi:10.3389/fphy.2019.00199

9. Centeno R, Mandon J, Cristescu SM, Harren FJM Three mirror off axis integrated cavity output spectroscopy for the detection of ethylene using a quantum cascade laser. *Sensors Actuators B-Chem* (2014) 203:311–9. doi:10.1016/j.snb.2014.06.122

10. Zheng K, Zheng C, He Q, Yao D, Hu L, Zhang Y, et al. Near-infrared acetylene sensor system using off-axis integrated-cavity output spectroscopy and two measurement schemes. *Opt Express* (2018) 26:26205–16. doi:10.1364/OE.26.026205

11. Leen JB, Yu XY, Gupta M, Baer DS, Hubbe JM, Kluzek CD, et al. Fast *in situ* airborne measurement of ammonia using a mid-infrared off-axis ICOS spectrometer. *Environ Sci Technol* (2013) 47:10446–53. doi:10.1021/es401134u

12. Mchale LE, Hecobian A, Yalin AP Open-path cavity ring-down spectroscopy for trace gas measurements in ambient air. *Opt Express* (2016) 24:5523–35. doi:10.1364/OE.24.005523

13. Nixon CA, Temelso B, Vinatier S, Teanby NA, Bézard B, Achterberg RK, et al. Isotopic ratios in Titan's methane: measurements and modeling. *Astrophys J* (2012) 749:159. doi:10.1088/0004-637X/749/2/159

14. Chen Y, Lehmann KK, Kessler J, Lollar BS, Couloume GL, Onstott TC Measurement of the 13 C/12 C of atmospheric CH4 using near-infrared

15. (NIR) cavity ring-down spectroscopy. *Anal Chem* (2013) 85:11250–7. doi:10.1021/ac401605s

15. Witinski MF, Sayres DS, Anderson JGHigh precision methane isotopologue ratio measurements at ambient mixing ratios using integrated cavity output spectroscopy. *Appl Phys B* (2011) 102:375–80. doi:10.1007/s00340-010-3957-2

16. Liu W, Tang M, Liu L, Lu X, Luo C Analysis and simulation of extracting radar modulation signal based on CIC filter. *IOP Conf Series: Mater Sci Eng* (2019) 569:032058. doi:10.1088/1757-899X/569/3/032058

17. Trudeau M, Chen P, Garcia G, Hollberg LW, Tans PP Stable isotopic analysis of atmospheric methane by infrared spectroscopy by use of diode laser difference-frequency generation. *Appl Opt* (2006) 45:4136–41. doi:10.1364/AO.45.004136

18. Abe M, Kusanagi S, Nishida Y, Tadanaga O, Takenouchi H, Sasada H Dual wavelength 3.2-μm source for isotope ratio measurements of $^{13}CH_4/^{12}CH_4$. *Opt Express* (2015) 23:21786–97. doi:10.1364/OE.23.021786

19. Zhang Z, Pang T, Sun P, Xia H, Li Z, Yu R, et al. Measurement of carbon isotope of methane and analysis of its genesis type using laser absorption spectroscopy. *Chin J Lasers* (2019) 46:1211001. doi:10.3788/CJL201946.1211001

20. Gordon IE, Rothman LS, Hill C, Kochanov RV, Tan Y, Bernath PF, et al. The HITRAN2016 molecular spectroscopic database. *J Quant Spectrosc Radiat Transfer* (2017) 203:3–69. doi:10.1016/j.jqsrt.2017.06.038